

A deterministic model for forecasting long-term solar activity

Eleni Petrakou*

Center for Axion and Precision Physics Research, Institute for Basic Science (IBS),
Daejeon 34141, Republic of Korea

February 2, 2017

Abstract

The successive long-term increase and decrease in Sun's activity associated with solar cycles has not been connected to a definite underlying mechanism so far, hence predictions about its amplitude usually depend on extrapolation from the sunspot number of previous cycles or observations of the geomagnetic field, becoming available only very close to or after a cycle's start and often departing from the actual events. Here we present a phenomenological model for quantitative description of the cycles' characteristics in terms of the number of M-class flares. The main element of the model is the relative ecliptic longitude of the planets Jupiter and Saturn. Using as input the temporal distribution of M-class flares during cycle 21, we obtain distributions for cycles 22-24 in notable agreement with the observed ones. Elements of shorter-term description can be elaborated further, however we are able to provide predictions for the evolution of solar activity for the rest of cycle 24 and for cycle 25. This deterministic description could contribute to elucidating the underlying physical mechanism and forecasting space weather.

Contents

Introduction	2
1 Observations and conventions	3
2 The model	5
2.1 Jupiter-Saturn approach and coupling to the 11-year modulation	6
2.2 Timing of the 11-year modulation	10
2.3 Angular range of activity	13
2.4 Summary of the model	14

*E-mail: petrakou@ibs.re.kr

3	Forecasting cycles 24 and 25	15
4	Further discussion	17
4.1	Other planetary effects	17
4.2	Historical activity	17
4.3	On physical mechanisms	18
5	Conclusions	19
	Bibliography	19
	Appendices	21
A	Performance and statistical testing	21
A.1	Performance	21
A.2	Timing	22
B	Systematic uncertainties	24
B.1	Binning effects	24
B.2	Fluctuations of the established length	25
B.3	Synodic period without adjustment	26

Introduction

Although the characteristic repetition in solar activity approximately every 11 years is apparently connected to the Sun's magnetic field, no definite underlying mechanism has been established; predictions about the amplitude of solar cycles usually depend on extrapolation from the sunspot number of previous cycles[1] or indirectly on observations of the geomagnetic field[2], becoming available only very close to or after a cycle's start[2, 3, 4] and often departing from the actual events. A comprehensive overview of solar cycle research and prediction methods can be found in [5]. Both short-term activity, e.g. solar storms, and its long-term evolution in cycles affect terrestrial events, including telecommunications and global climate.

Here we present a phenomenological model for the quantitative description of individual cycles' features, such as start, intensity, evolution, in terms of the number of M-class solar flares. Motivated by the recent work in [6], which reported correlation between the eruption of solar flares and the positions of the four inner planets, we extend relevant notions with the inclusion of the two gas giant planets, the use of relative instead of absolute positions, and the focus on long-term solar activity. The main factor of the model is the relative ecliptic longitude of the planets Jupiter and Saturn. Using as input the data of cycle 21 we are able to reconstruct satisfactorily the latest three cycles and provide predictions for the next years.

Section 1 describes the used observations and their treatment. Section 2 presents the details of the model, which comprises of two main components. Section 3 provides predictions for the rest of the current cycle and the next one. Section 4 discusses briefly further points (effects related to the other planets, past activity, and bibliography on possible underlying physical mechanisms). Conclusions are found in Section 5. In addition, Appendix A presents performance and statistical tests of the model, while Appendix B gives details about the sources of systematic effects and their derivation.

1 Observations and conventions

Solar flares

Sunspots are darker areas on Sun's surface, corresponding to reduced local temperature, caused by concentrations of magnetic field flux; their typical lifetime is in the order of days. Solar flares occur from abrupt release of magnetic energy and are related to sunspots since they both occur in magnetically active regions of the corona; the emission from flares spans the whole electromagnetic spectrum and includes massive particles, with duration in the order of minutes. While studies of the solar cycle traditionally use the sunspots as observable, here we will employ solar flares, following the work in [6]: While sunspots are indirect indicators of underlying dynamics, flares are actual physical events with definite timing and released energy, as well as real impact on space weather. The obvious drawback is being constrained to examining the four latest cycles, for which solar flare records exist.

Solar flares are categorized on a logarithmic scale according to their X-ray brightness. The top three categories are known as X-class, M-class and C-class, in decreasing order, with M-class spanning 10^{-5} - 10^{-4} W/m². At the present stage of this study only the solar flare counts are used without considering their intensity; this treats the occurrence of flares as statistical timed events. Typically, X-class flares are rare while C-class flares occur almost daily, therefore we restrict the sample to M-class flares, since their emergence involves less randomness than C-class while they comprise a larger statistical sample than X-class flares. Both intensities and all flare classes are planned to be examined at a next stage of this work.

Since the start of cycle 21 up to the end of year 2016 there have been 6,332 M-class flares (Fig.1). The count for each cycle is quoted in Table 1. The data are X-ray flux measurements of the NOAA SMS and GOES satellites[7]. In order to have an exact overview of the effects under discussion no smoothing is applied on the distributions, other than the binning in histograms.

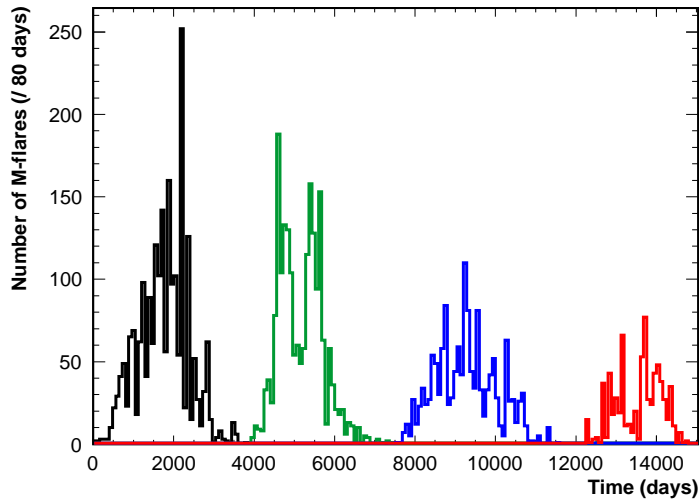


Figure 1: *Number of M-class flares as a function of time, for solar cycles 21-24, starting on 1976/08/18. Each cycle is plotted in a different colour. Each bin spans 80 days. The end of year 2016 is found at day 14,894.*

Table 1: *Number of flares and start months of the last four solar cycles (see text for definition of start dates).*

Solar cycle	Number of M-class flares	Start month	Duration (days)
21	2,175	Aug 1976	3,882
22	2,021	Apr 1987	3,649
23	1,434	Apr 1997	4,676
24	702 (ongoing)	Jan 2010	2,537 until end of 2016

Timing convention

We will define the start of each cycle by the appearance of the first flare erupting from a sunspot with reversed magnetic polarity. The end of each cycle is defined by the start of the next one. The resulting dates and durations are found in Table 1.

In some of the following all four cycles will be plotted on a common time scale (Paragraph 2.1). For this, the temporal middle of each cycle is placed on zero, the axis is expanded

from -2,000 to 2,000 days, and the data are plotted individually for each cycle. The date for the middle of the ongoing cycle 24 was determined by the calculation described in Paragraph 2.2, which comprises one of the elements of the model.

The individual distributions have short-scale differences with respect to Fig.1, due to the different start values of the bins; the systematic uncertainty resulting from the binning choices is taken into account in the analysis (Paragraph 2.1 and Appendix B.1).

Convention for the relative angle of the two planets

In the rest of the text, the relative heliocentric ecliptic longitude between Jupiter and Saturn will be used frequently. All quoted angles will refer to the two planets' relative ecliptic longitude, with either conjunction or opposition corresponding to zero degrees, i.e. both cases of alignment are treated equivalently.

For illustration, if Jupiter is found at 30° ahead of Saturn then the relative angle is $+30^\circ$ (Fig.2, case a), while if it is at 345° ahead of Saturn then the relative angle is -15° (Fig.2, b). If Jupiter is found at 160° ahead of Saturn then the relative angle will be -20° (Fig.2, c), since they are approaching their next closest alignment, which will be the next opposition. Consequently, the range of values of the relative angle is $[-90^\circ, 90^\circ]$. Note that, for instance, “91°” is actually -89° , since the closest alignment is the next opposition.

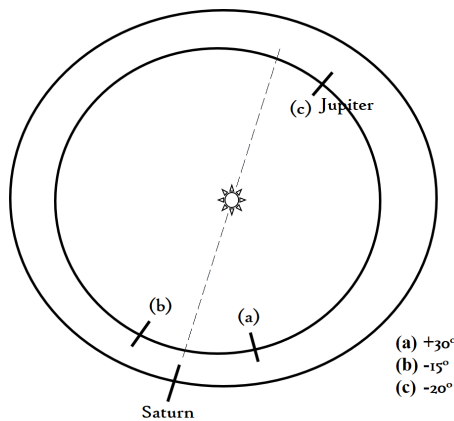


Figure 2: *Examples for the relative angle between the two planets according to the convention used in the text.*

2 The model

This study focusses on the general features of solar cycles -such as start, duration, intensity, overall development- in terms of the number of M-class flares (“flares”), bypassing short-time structures. We will demonstrate that such features can be described in a deterministic way by a model consisting of two elements, presented in Paragraphs

2.1 and 2.2. Some additional points are discussed in Paragraph 2.3, with a brief wrap-up in Paragraph 2.4.

2.1 Jupiter-Saturn approach and coupling to the 11-year modulation

The principal component of the model is an apparent coupling between the empirical 11-year range associated with solar cycles (“established” range) and the relative angle between Jupiter and Saturn (“the two planets”). Such an effect could be the manifestation of an internal solar mechanism with an external planetary trigger, however no speculations are made at present about its nature.

More precisely, we propose that *the main drive behind the evolution of solar activity is strongly correlated to the relative ecliptic longitude of Jupiter and Saturn; however, this effect can only act within the constraints of the established 11-year range.*

In this Paragraph, these two contributions will be quantified by using two distributions extracted from the observations. Since these two quasi-periodic contributions have different lengths¹, their combined effect changes with time; we are going to quantify their coupling by displacing them appropriately and obtaining their common area. We will then demonstrate that the distribution of this overlap area can describe the global characteristics of the solar cycles to a satisfactory degree.

The quantification of this proposition starts with certain assumptions:

- The effect of each of these two contributions on the solar activity follows a Gaussian distribution.
- Both contributions are equally strong, therefore the two distributions have the same maximum height.
- Empirically, the established range spans roughly 11 years. When the two planets’ relative longitude is considered, then activity is observed to be stronger mainly within the range of -45° to $+45^\circ$ around their alignment (Fig.3).

Using these assumptions, corresponding distributions will be extracted from the observations.

The Gaussian distributions

We aim to obtain the two distributions described above, one corresponding to the Jupiter-Saturn approach and one corresponding to the established “11-year” period.

¹The established contribution fluctuates around approximately 11.0 years. The Jupiter-Saturn synodic period oscillates around its average of ~ 19.9 years, with alignments found at half this length.

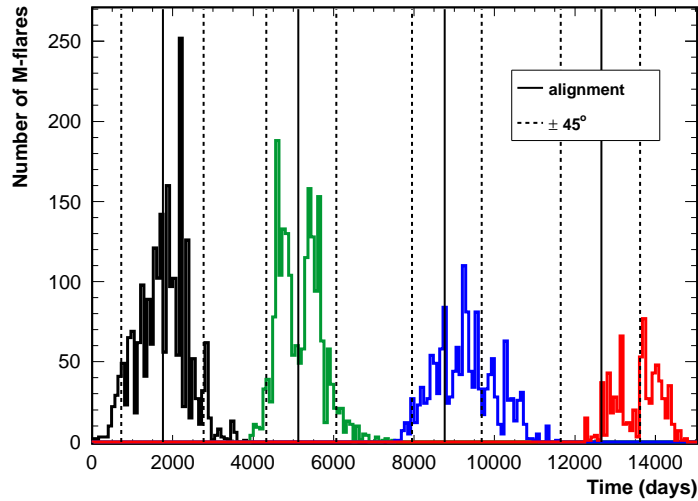


Figure 3: *Distribution of flares for the last four cycles, with guides plotted at -45° , 0° and $+45^\circ$ of the two planets' relative angles.*

For this we will use cycle 21 where, by a useful coincidence, the two planets' conjunction took place only 238 days before the middle of the cycle: Therefore we will assume that in cycle 21 the deployment of both effects in their full ranges can be seen, and the two distributions can be obtained by fitting the data.

The assumptions made about the two effects are translated into the following requirements about the Gaussian functions:

- One of the Gaussians is centered on the middle of the cycle, and the other is centered on the date of the Jupiter-Saturn alignment.
- Both functions have the same constant.
- Their $\pm 2\sigma$ ranges roughly cover, respectively, 3,000 days and between the dates of -45° to $+45^\circ$ around the alignment.

It must be noted that in this case minimization of the fitting function's parameters is not the most suitable approach, because of the intense small-scale fluctuations in the solar activity. What was preferred was a quasi-empirical modelling, by still using minimization², but constraining the fitting ranges so as to result in a satisfactory description of the data.

Accordingly, the means of the distributions were fixed on the corresponding dates, while the ranges for the constant and the standard deviation were constrained as described above. The fit for the Jupiter-Saturn Gaussian was performed first, and the obtained

²With the MINUIT[8] module in the ROOT[9] analysis package.

value for the constant was subsequently fixed in the fit for the “11-year” Gaussian. The two resulting functions are shown in Fig.4. Their parameters are given in Table 2.

A systematic uncertainty of 13.5% was assigned to the model because of effects from the binning choices (not shown in Fig.4, shown later in Fig.7). Appendix B.1 gives details about its derivation.

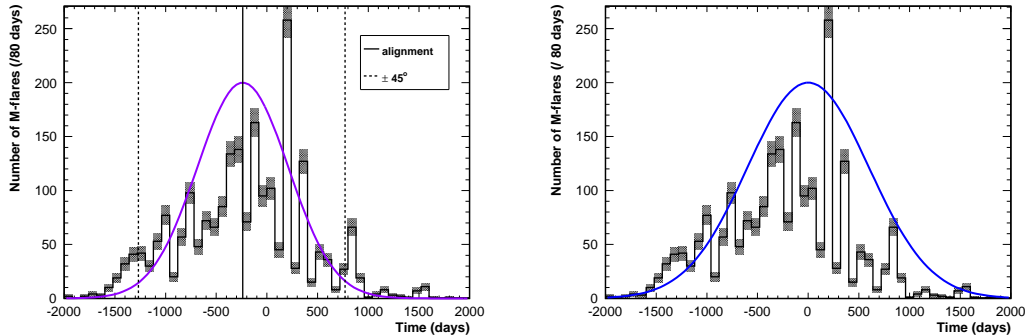


Figure 4: *Distribution of flares for cycle 21 and fitting results for the Gaussian functions corresponding to the Jupiter-Saturn effect (left) and to the “11-year” effect (right). Each bin spans 80 days. In the case of the Jupiter-Saturn effect, guides are plotted at -45° , 0° and $+45^\circ$. (Poisson errors are shown on the data to illustrate the ranges used by the fitting algorithm.)*

Table 2: *Parameters of the two fitted Gaussians, for binning in 80 days. The Jupiter-Saturn mean refers to cycle 21.*

	constant	mean	st. deviation
“11-year” Gaussian	200	0	600
Jupiter-Saturn Gaussian	200	-238	450

Coupling

After obtaining the two distributions corresponding to the two considered effects, the next step is to center the Jupiter-Saturn Gaussian on the date of the two planets’ alignment *in each cycle*. In all cases, the center of the “11-year” Gaussian corresponds to the temporal middle of the cycle. It should be stressed that, for all cycles, the two functions used are those obtained from the fit on cycle 21 with the only changing parameter being the date on which the Jupiter-Saturn Gaussian is centered. (The determination of the middle of the ongoing cycle 24 is derived from the second component of the model, which is explained in the next Paragraph, 2.2.)

As mentioned above, we propose that the area of overlap of the two Gaussians can describe the coupled effect of these two contributions. This is plotted in Fig.5 individually for each cycle; the left-hand plots show the two distributions, while their common area

is plotted in the right-hand plots, with the same binning as for the data. *The latter distribution quantifies the two contributions and their coupling, and is the first element of the model.*

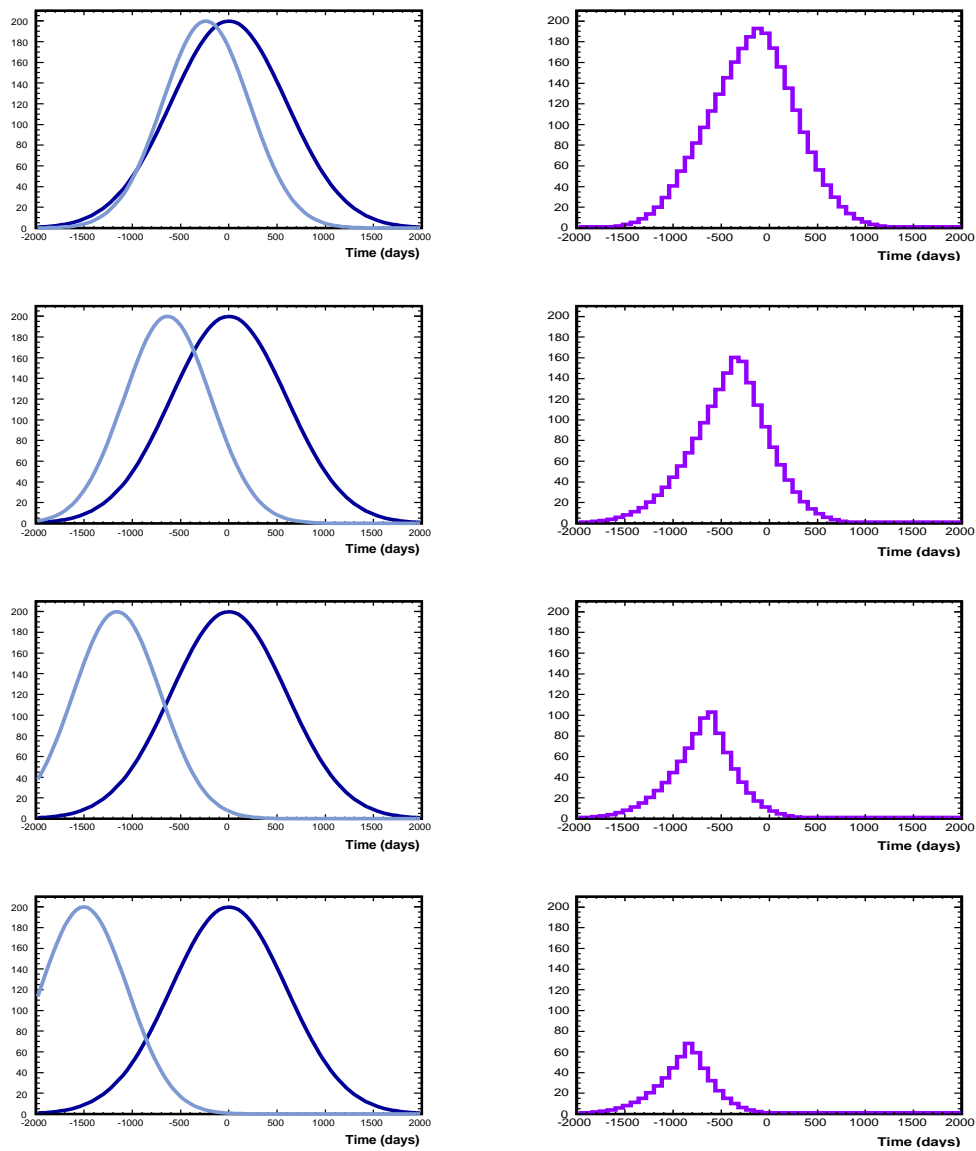


Figure 5: From top to bottom: Cycles 21 to 24. Left column: Placement of the two Gaussians for each cycle, with the center of the “11-year” distribution (blue) corresponding to each cycle’s temporal middle, and the center of the Jupiter-Saturn distribution (light blue) placed on the respective dates of alignment. Right column: The binned overlap area of the two distributions.

Comparison to data

As the last set of histograms (Fig.5, right) is expected to form the main part of our model, the data is overlaid on them for comparison in Fig.6. For better overview, the same result is plotted on a common time axis in Fig.7, and including the used Gaussian distributions in Fig.8.

For completeness: The plot for cycle 23 has 26 underflow events. For more clarity no uncertainties are shown in Fig.6, but they are plotted in Fig.7. The statistical uncertainty is the Poisson error on the predicted number of flares per bin. The systematic uncertainty comes largely from the binning effects, with the derivation discussed in Appendix B.1 (it also includes a smaller uncertainty related to the calculations in Paragraph 2.2, whose derivation is found in Appendix B.2).

The model appears to be in noticeable agreement with the data on the timing, intensity and evolution of activity in each cycle, and also roughly on the total span. However, it is not predictive yet since it requires knowledge of the date of each cycle's middle, which was obtained from observations. The next Paragraph deals with this point.

2.2 Timing of the 11-year modulation

In the following it is proposed that the duration of each cycle is directly related to the time span between consecutive Jupiter-Saturn alignments, and therefore the middle of the cycle, on which the “11-year” Gaussian is centered, can be known in advance.

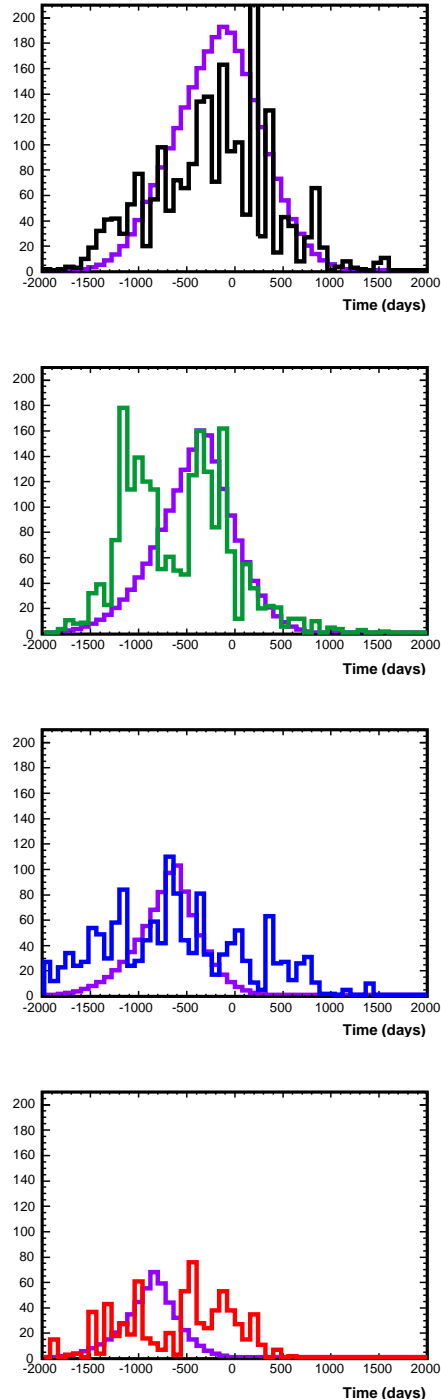


Figure 6: *From top to bottom: Cycles 21-24. Overlap area of the two Gaussian functions (purple), overlaid with the data from each cycle.*

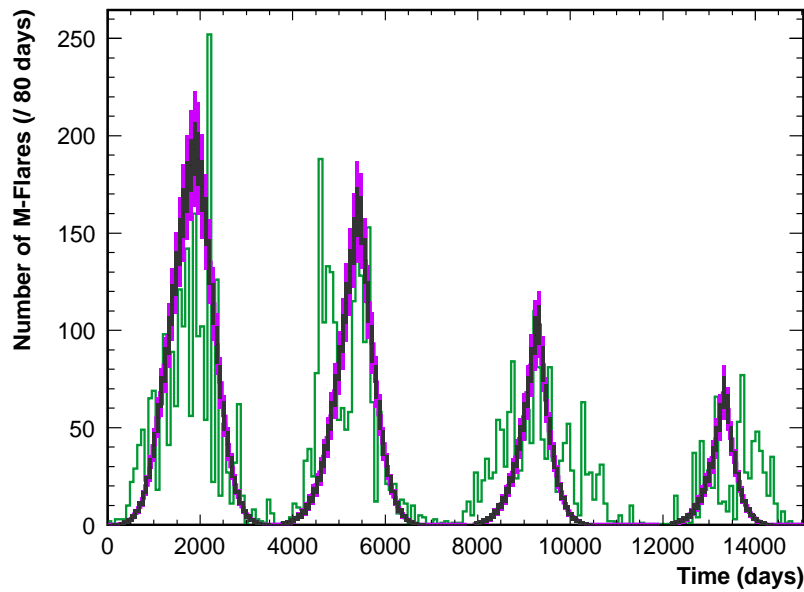


Figure 7: All flare observations for the last four cycles (green), overlaid with the prediction distributions. The prediction includes statistical uncertainty (gray) and systematic uncertainty (violet). (The end of year 2016 is found at day 14,894.)

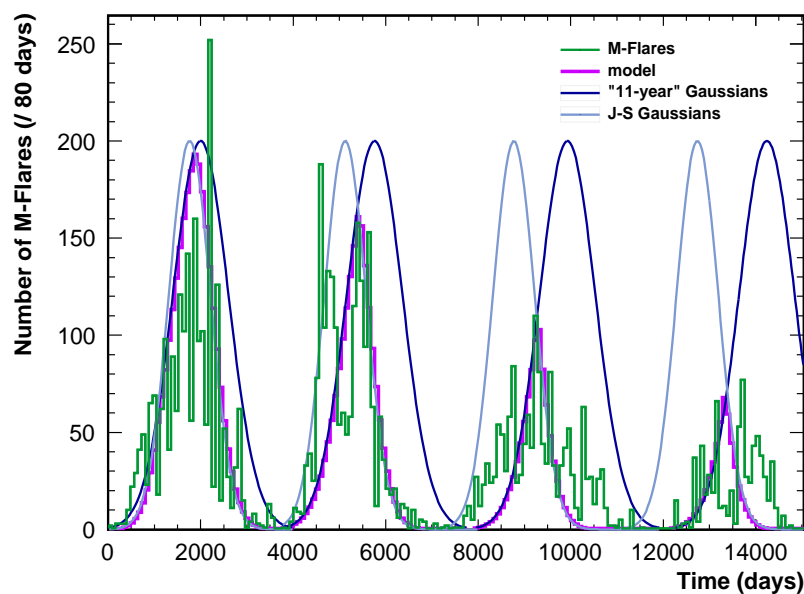


Figure 8: Data overlaid with the two types of Gaussians and the prediction distributions resulting from their overlap. (No uncertainties are plotted.)

The average time length between Jupiter-Saturn alignments is 9.95 years (3,634 days), with a natural oscillation within 2%. The established duration of the solar cycle fluctuates around 11.02 years (4,025 days), with a recorded deviation of 10%. (It must be noted, however, that using as exact a number as 4,025 might be larger precision than should be used: The sample of documented cycles is rather small, their durations vary strongly, and the calculation is affected by determining the cycles' starts from the sunspots' field reversal instead of the onset of flares³.)

As a result of the different lengths of the two contributions, the displacement between the middle of a cycle and the two planets' alignment is increased by ~ 391 days on average between consecutive cycles. The actual increase in the displacement between cycles 21 and 22 was 398 days, and between cycles 22 and 23 it was 523 days. Table 3 quotes the displacements and the difference of their increase from its average. The Table also lists the lengths between the consecutive Jupiter-Saturn alignments in cycles 21-24, and their difference from their average value of 3,634 days. (In the following, "displacement" refers to the time between the temporal middle of a cycle and the date of the preceding alignment.)

Table 3: *Displacement, time between alignments, and related differences from average values.*

(all numbers in days)	Displacement between cycle's middle and J-S alignment	Difference between the increase in consecutive displacements and its average value (391)	Time length between consecutive J-S alignments	Difference between the J-S time length and its average value (3,634)
Cycle 21	238	(n/a)	3,367	-267
Cycle 22	636	7	3,640	6
Cycle 23	1,159	132	3,897	263

In this case the "data sample" consists of only two pairs of cycles, however a hypothesis could still be made: The increase in the displacement follows the time length between two successive alignments. Indeed, the former differs from its average value by half the difference of the length between consecutive alignments in cycle 23, while for cycle 22 they both have values small enough to be compatible with this hypothesis. (The displacement refers to half a cycle, while the time between alignments refers to a full cycle, thus the factor of one half.)

Put concisely, the displacement in a cycle actually differs from its average value, by the amount of time that the length of the two corresponding successive alignments differs from its own average (columns three and five respectively in Table 3). From this, the placement of the "11-year" Gaussian is determined, and the total length of a cycle follows.

³Parenthetically, for cycles 21-23 the average duration calculated from sunspots is 10.6 ± 0.7 years, and with the definition using flares it is 11.1 ± 1.2 years.

This statement can be put in the form of a simple expression:

$$[displacement] = D + (\langle 11y \rangle - \langle L_{JS} \rangle) + \frac{L_{JS} - \langle L_{JS} \rangle}{2} \quad (1)$$

where D is the displacement in the previous cycle, $11y$ is the established length, and L_{JS} is the time length between the alignment in the examined cycle and the next one; brackets denote the average value of the two time lengths, which is equal to 391 and 3,634 respectively.

The next alignment will take place 3,541 days after the last one, therefore by applying Eq.1 the middle of cycle 24 is found to be at 1,503 days after the latter, on 7th April 2015. This date was used for centering the “11-year” Gaussian in the plots of the previous Paragraph. It follows that the length of cycle 24 is calculated to be 3,808 days, i.e. lasting up to June 2020. At this point the model can be considered fully predictive, as it does not require any input for the calculations, other than the distribution of cycle 21.

For completeness: The middles of cycles 22 and 23 as calculated by this expression fall 4 days before their actual dates; since the difference is small compared to the bin size (80 days), the plots of the previous Paragraph hold. Also, it is obvious that as the alignments move forward with respect to the cycles’ middles, at some point *two* Jupiter-Saturn Gaussians will enter an “11-year” Gaussian. Our dataset did not happen to include this case, but it is examined further in Paragraph 3.

A systematic uncertainty in the increase of the displacement is introduced from the dispersion of the “11-year” length around its average, which is propagated to the relative centering of the two Gaussian distributions. Its derivation is discussed in Appendix B.2. This uncertainty is applied whenever Eq.1 is used for the calculation of the date for centering the established Gaussian. Fig.7 also included this systematic effect, whose magnitude can be seen separately in Appendix B.2 (Fig.16).

Lastly, the relation between the evolution of solar activity and the displacement, with the latter actually acting as a measure of the two contributions’ coupling, can also be illustrated by Fig.9: Although the placement of the “11-year” Gaussian and the resulting modelling concern mainly the *central* part of each cycle, the *total* number of observed flares in each cycle is plotted in this case as a function of the displacement.

2.3 Angular range of activity

Although no physical mechanism is inferred yet, phenomenologically the solar activity seems to be regulated by the approach and retreat of the two gas giants, with conjunction and opposition having equal roles. In this picture, when the two planets start approaching to their alignment closer than -90° , a build-up of activity begins which manifests after some further approach. When the planets move away from alignment the activity starts to decrease, following however the pattern of the overlap with the established

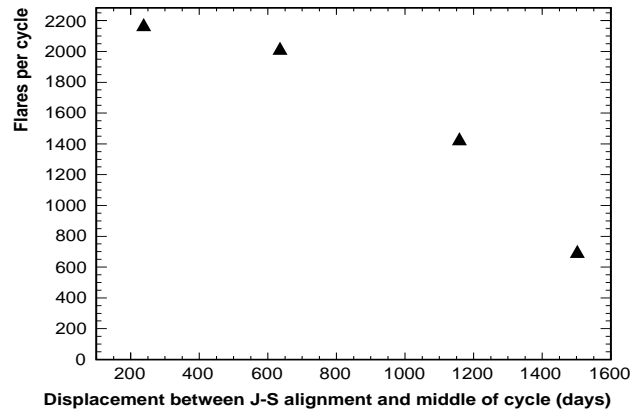


Figure 9: *Total number of flares observed in each cycle, as a function of the displacement between its middle and the previous Jupiter-Saturn alignment.*

contribution. Finally, when they retreat further away than $+90^\circ$, the activity dies off as a new phase of approach to the next alignment actually begins.

The compatibility of this scenario to the observations can be seen in Fig.8, where the dates of $|90^\circ|$ are found at the edges of each Jupiter-Saturn Gaussian. A notable case seems to be the ongoing cycle. Several prediction methods, even updated as late as 2009, expected smoothly decreasing activity in 2016 and later[3]. In reality the solar activity almost disappeared after the retreat further than $+90^\circ$ in December 2015, with only a handful of M-class flares in 2016 and even 32 spotless days.

Although the model agrees with the main part of the cycles in the overall intensity and timing, time ranges outside the overlap are not covered by it. However, wherever both Gaussians still have significant strength, these ranges are seen to host activity of intensity comparable to the main part. This point is left to be quantified in a subsequent stage of the analysis. (At any rate, some relevant discussion is found in Paragraph 3.)

2.4 Summary of the model

A quantitative model was presented for the description of the solar cycles in terms of M-class flares activity. Although no proposal is made yet about the underlying physical mechanism, the activity was found to be significantly modulated by the relative motion of Jupiter and Saturn.

More specifically, it is stated that: *The main drive behind the long-term solar activity is strongly correlated to the approach and retreat of Jupiter and Saturn with respect to their alignments. Every new phase of activity starts as they approach closer than 90° of relative ecliptic longitude. However, this effect can only act within the bounds of the “established” 11-year periodic range.*

We were able to quantify these observations by using two components:

- The combined effect of the two modulations, as quantified by the overlap of two Gaussian functions extracted from the data of cycle 21⁴.
- The determination of any cycle’s temporal middle, derived from the average length of the established modulation and the exact length between consecutive alignments of the two planets.

In addition, it is observed that, outside the overlapping area, activity is expected in ranges where both Gaussians still have significant strength, with a decrease towards the date of $+90^\circ$ which separates phases of activity.

The sole input to the model is the temporal distribution of flares in cycle 21 and the date of its middle. Forecasting for other cycles can be done by using the dates of the two planets’ alignments. The next Section provides predictions for the rest of cycle 24 and for cycle 25.

Quantification and tests of the model’s descriptive strength are presented in Appendix A.1. Additional tests in Appendix A.2 probe the possibility that a satisfactory description can emerge randomly from using the specific Gaussian distributions. Both kinds of results provide supplementary support for the proposed mechanism.

3 Forecasting cycles 24 and 25

In order to discuss about the evolution of the rest of the current and the next solar cycle, the two types of Gaussians are plotted in Fig.10 for the next years, centered on the appropriate dates as described in Paragraph 2.2.

According to the model as described in Section 2.1, activity is expected in the large overlap region around day 19,000, following the actual shape of the overlap distribution. This will form essentially the main part of cycle 25, which would be rather brief as the next “11-year” period will be reaching its end. Its intensity will be comparable to that of the current cycle.

⁴A note concerning the fit constraints: If we perform an unconstrained minimization fit on cycle 21, the result has a height of around 100, deviation around 500, and its mean is moved to the left; the values for the other two parameters persist if the mean is placed either on the cycles’ middle, the alignment date or the “local maximum” bin with 160 flares.

A similar result is obtained if we drop the assumption that the two Gaussians have the same height: Then the minimization arranges both heights so that in the overlap area we see only the distribution from the Jupiter-Saturn Gaussian with its height changed to ~ 100 . Therefore, in both cases it can be said that unconstrained fits result in a “trivial Gaussian”, which does not describe satisfactorily the data.

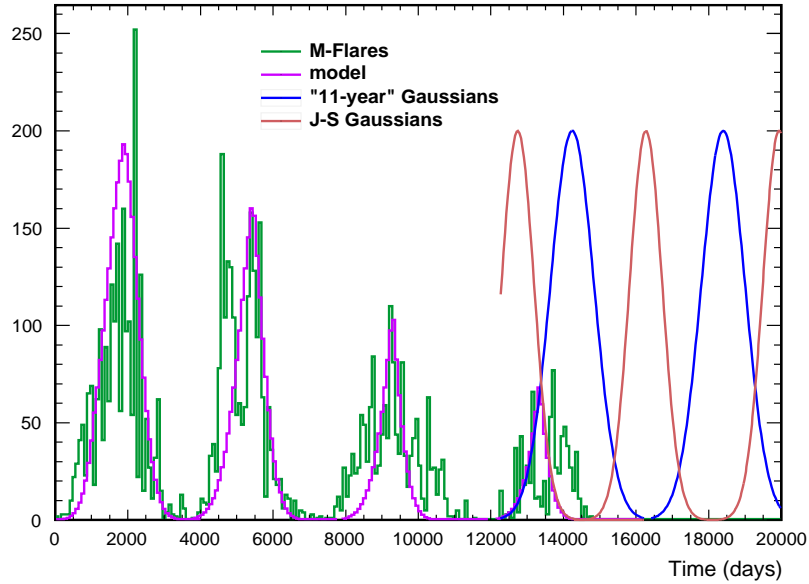


Figure 10: *Flare observations and model distributions, with the two types of Gaussians expanded over the next $\sim 5,000$ days, starting from cycle 24. (The end of year 2016 is found at day 14,894.)*

However, as discussed in Paragraph 2.3, activity is also expected empirically inside other time ranges where both Gaussians have significant strength (although this point is not quantified so far). Accordingly, activity could appear in the first two smaller overlap areas.

In between the three overlap ranges no notable activity is expected, since we are at the fringes of the established modulation (in the first instance) and around 90° of the Jupiter-Saturn modulation (in the second instance).

The overall picture is compatible with the current “orthodox” expectation of a minimum in solar activity (which is, however, mainly the result of extrapolations from the previous cycles). Features similar to the Dalton minimum could be expected.

In addition to the intensity and duration of activity, another feature is the transition from a cycle to a new one. A new solar cycle is traditionally defined by sunspots with reversed magnetic field and, under our scheme, flares erupting from such sunspots. As the established modulation is reasonably considered to be the determining factor here, field reversal is expected to occur in the second overlap area. (In this case, cycle 24 could be characterized by triple peak activity. This point could even be settled around the end of 2017/start of 2018, after some advancement into the first overlap area.)

4 Further discussion

4.1 Other planetary effects

The findings reported in [6], suggesting a relation between short-term evolution of solar activity and the inner planets' positions, can be viewed complementarily with those here. A common description can underlie phenomena of different time scales, with a higher-frequency modulation due to the fast-moving planets closer to the Sun and a more stable long-term element (the solar cycle) due to the massive and slower gas giants.

As to planets Uranus and Neptune, although their distance from the Sun makes their contribution appear unlikely, their slow motion can conceivably add a steady underlying element in very-long-scale solar activity. A brief observation can be made about their possible role: During the recorded solar history three conjunctions of Uranus and Neptune took place, in the years 1650, 1821 and 1993. With a first look these dates are in the vicinity of the three extrema of recorded activity: The Maunder minimum between years 1650 and 1710, the Dalton minimum in 1800-1820, and the modern maximum in the end of the 20th century. However these obviously include both minima and maxima.

Nonetheless, a distinguishing feature exists between these cases. Close to the minima, the corresponding Jupiter-Saturn alignments occurred at a normal angle with respect to that of Uranus and Neptune, while in the case of the maximum Jupiter and Saturn were aligned also with Uranus and Neptune. Notably, just before the Maunder minimum two consecutive Jupiter-Saturn alignments were actually covered, both at a normal angle with respect to the Uranus-Neptune conjunction.

These concepts remain to be quantified, but a combined effect of this kind is a plausible extension of the mechanism described for Jupiter and Saturn. If present, then the Maunder minimum could be the result of a significant disruption in the solar activity pattern, since the formation of two consecutive cycles was affected. As about the modern maximum, it could point to the fact that the global upper "bound" of solar activity, which was taken as a given factor in this model, is actually regulated by a synergy between the four outer planets.

4.2 Historical activity

An extrapolation of the model back to the whole era of reliable sunspot records and comparison to the sunspots activity could be informative, although there are expected sources of discrepancy: The standard representation of sunspot activity is smoothed to its 13-month mean, the model presented here is not definitive yet on the cases with two Jupiter-Saturn Gaussians entering a single "11-year" Gaussian, and more importantly, a precise correspondence between sunspots and flares activity is not established in general. Moreover, a complete description should obviously be extended to all possible planetary effects, as discussed briefly in the previous Paragraph.

At any rate a simplistic extrapolation of the model is shown in Fig.11; dots correspond to the maximum height of the main area of overlap between the two Gaussians in each cycle, and exhibit rough compatibility with the sunspot maxima and general evolution, but displacement in the timing of the minima. More detailed comparison is one goal of the next stage of the analysis. The establishment of a correspondence between the two solar indices and the consideration of all planetary effects should be parts of such a comparison.

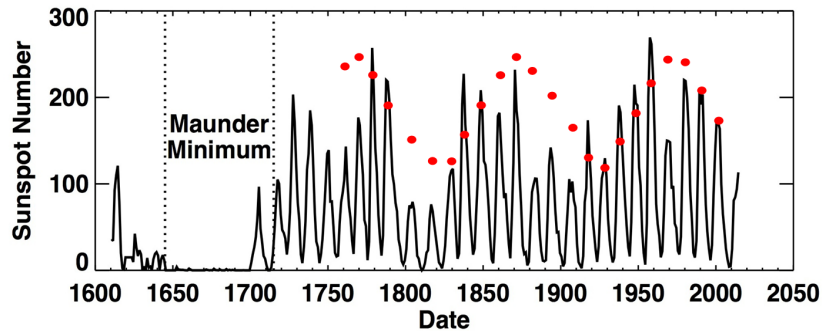


Figure 11: *Extrapolation of the model (red) to the whole era with sunspot records, overlaid with the historical observations (smoothed sunspot monthly averages). The values of the model are normalized to the peak of cycle 23. (Image credit: Marshall Space Flight Center/NASA.)*

4.3 On physical mechanisms

Energetic solar events and the solar cycle are widely attributed to a magnetic dynamo mechanism[10] although their modelling is still far from complete[11] and no internal or external regulating factors have been established. Over the past two centuries a number of studies have occasionally pointed out relations between the planets' periods and solar activity; although planetary tidal effects have been disfavoured[12], other possible explanations have been put forth. However, most of the relevant work is based on spectral analysis or pure arithmetic analysis of patterns in solar activity and planetary periods, with only a few studies attempting quantification using timed solar weather events.

We list indicatively some notable recent studies, while pointing out that the discussion is open on several of them. A planetary torque exertion on the tachocline is examined in [13]; the spectral analysis in [14] focusses on the combined effects of Jupiter and Saturn, while [15] focusses on Uranus and Neptune and discusses a spin-orbit coupling mechanism. The latter builds on a proposal based on the motion of the solar system's barycenter [16], which was elaborated recently also in [17] with findings of some similarity to those presented here. It is perhaps noteworthy that all these studies point to a coupling between an internal mechanism and external triggers.

A proposal of different nature is the lensing of dark matter streams[18] in [6], where relation between planetary positions and solar flares was first reported. A recent study with findings similar to [6] concerning the role of the inner planets is presented in [19].

Finally, a remarkable phenomenological study is [20], which directly related planetary positions with terrestrial radio propagation conditions.

At this stage of the present work no inferences are drawn about possible underlying mechanisms. However this modelling, and any further quantification of it, is expected to offer definite hints for their determination.

5 Conclusions

A model was presented for the phenomenological description of long-term solar activity and the quantification of the main features of solar cycles. The principal element of the model is a coupling between the empirical time length of ~ 11 years and the relative ecliptic longitude of the planets Jupiter and Saturn. This coupling was expressed by the common area of two Gaussian distributions, both extracted from the observations of M-class flares in solar cycle 21.

An element required by this modelling is the date of a cycle's temporal middle; this is calculated from the time lengths of the two involved effects, i.e. the ~ 11 -year length and the time between consecutive alignments of the two planets.

Thereby, using as input the observations of cycle 21 we reproduce the distributions of activity in the latest three cycles to a satisfactory degree. The model is extended to the next years, providing predictions for the rest of cycle 24 and cycle 25.

This model describes mainly the central part of the cycles, with phenomenological propositions about the outer ranges remaining to be quantified in subsequent steps of the analysis. Other planned optimizations include the use of the flares' intensity and other X-ray classes, and precise comparisons to historical records.

Although no proposal is made about the underlying physical mechanism, these results point strongly to a correlation between the triggering of solar activity and the relevant position of the gas giants, with the activity increasing and declining respectively with their approach and retreat. While numerical relations between the time lengths involved in these effects have been noticed in the past, they were not quantified by using actual solar events. The present results and further quantification are expected to contribute to the understanding of the mechanisms involved in solar dynamics, and they could be employed in long-term forecasting of space weather.

Acknowledgments

The author is indebted to Juan-Carlos Algaba, Jonghee Yoo, Kalliopi Iordanidou, Marios Maroudas and Jonathan Elkin for the useful discussions, and particularly to Konstantin Zioutas.

This work was supported by grant IBS-R017-D1-2017-a00 of the Republic of Korea.

References

- [1] D.H. Hathaway, R.M. Wilson, E.J. Reichmann, “The shape of the sunspot cycle”. *Sol. Phys.* 151, 177 (1994)
- [2] D.H. Hathaway, R.M. Wilson, E.J. Reichmann, “A synthesis of solar cycle prediction techniques”. *J. Geophys. Res.* 104, 22,375 (1999)
- [3] NOAA Space Weather Prediction Center. Solar Cycle 24 Prediction Updated May 2009. <http://www.swpc.noaa.gov/content/solar-cycle-24-prediction-updated-may-2009> (2009)
- [4] D.H. Hathaway, R.M. Wilson, “Geomagnetic activity indicates large amplitude for sunspot cycle 24”. *Geophys. Res. Lett.* 33, 18101 (2006)
- [5] D.H. Hathaway, “The Solar Cycle”. *Living Reviews in Solar Physics* 12, 4 (2015)
- [6] S. Bertolucci, K. Zioutas, S. Hofmann, M. Maroudas, “The Sun and its Planets as detectors for invisible matter”. *arXiv:1602.03666* (2016)
- [7] Archive of the Space Weather Prediction Center, USA National Oceanic and Atmospheric Administration. <http://www.swpc.noaa.gov>
- [8] F. James, M. Roos, “Minuit: A System for Function Minimization and Analysis of the Parameter Errors and Correlations”. *Comput. Phys. Commun.* 10, 343 (1975)
- [9] R. Brun, F. Rademakers, “ROOT - An Object Oriented Data Analysis Framework”. *Nucl. Inst. & Meth. in Phys. Res.* A389, 81 (1997)
- [10] E.N.Parker, “Hydromagnetic dynamo models”. *Astrophys. J.* 122, 293 (1955)
- [11] For example: H.C.Spruit, “Theories of the solar cycle: a critical view”, *arXiv:1004.4545* (2010)
- [12] C.M.Smythe, J.A.Eddy, “Planetary tides during the Maunder Sunspot Minimum”. *Nature* 266, 434 (1977)
- [13] J.A.Abreu et al, “Is there a planetary influence on solar activity?”. *A&A* 548, A88 (2012)
- [14] N.Scafetta, “Multi-scale harmonic model for solar and climate cyclical variation throughout the Holocene based on Jupiter–Saturn tidal frequencies plus the 11-year solar dynamo cycle”. *JASTP* 80, 296 (2012)
- [15] G.J.Sharp, “Are Uranus & Neptune Responsible for Solar Grand Minima and Solar Cycle Modulation?”. *IJAA* 3, 260 (2013)
- [16] P.D.Jose, “Sun’s Motion and Sunspots”. *AJ* 70, 193 (1965)

- [17] I.R.G.Wilson, B.D.Carter, I.A.Waite, “Does a spin-orbit coupling between the Sun and the Jovian planets govern the solar cycle?”. *Pub. of the Astr. Soc. of Australia* 25, 85 (2008)
- [18] K.Freese, P.Gondolo, H.J.Newberg, “Detectability of weakly interacting Massive Particles in the Sagittarius dwarf tidal stream”. *Phys. Rev. D* 71, 043516 (2005)
- [19] I.Edmonds, “Revisiting 154-day periodicity in the occurrence of hard flares. A planetary influence?”. *arXiv:1611.04240* (2016)
- [20] J.H.Nelson, “Shortwave radio propagation correlation with planetary positions”. *RCA Review*, XII, 1 (1951)

A Performance and statistical testing

The performance of the model on some of the main features of the cycles and its correlation with the data are examined in Paragraph A.1 (the tests have similarities to [2], where the main methods used in practice for the forecasting of solar activity were evaluated). In Paragraph A.2 it is tested whether a satisfactory agreement between the data and the overlapping of the two used Gaussians could arise randomly, or if it is indeed related to the two planets’ synodic period.

A.1 Performance

The performance of the model is tested by using the quantities listed below for describing some of the cycles’ main features in more specific terms. All comparison is between the observations and the distribution from the model (Fig.7). The bin with the global maximum of 252 flares in cycle 21 is excluded from all calculations in Paragraph A.1 as an outlier. In the following, “maximum count” will refer to the largest number of flares in a single bin within a specified range.

- Difference in maximum count within the range 0° - 45° ⁵ (measured in counts and in standard deviations).
- Distance of the positions of the maximum count within 0° - 45° (in bins).
- Difference in global maximum count (in counts and in deviations).
- Distance of the positions of the cycles’ start, as defined by the first bin with $\geq 5\%$ of the maximum count within 0° - 45° from data (in bins).

⁵The range 0° - 45° , the “central part” of the cycles, is described more accurately by the model by construction.

- Difference in the total length of cycle, as calculated with Eq.1 (in days).

The values of these quantities are given in Table 4. The standard deviation is calculated from the statistical uncertainty and all applicable sources of systematics (Appendix B.1, B.2).

In addition, the Pearson correlation coefficient between the distributions of flares from observations and from the predictions has the values 0.88 and 0.73, within 0° - 45° and in the whole range respectively (Fig.12). In both cases the p-value for this correlation arising by chance is smaller than 10^{-7} , as calculated from random permutation of the two sets of datapoints.

Table 4: Values for quantifiers of some of the cycles' main features, both for each cycle and for their RMS. The numbers are the absolute difference between the predictions and the data. Each bin of the two distributions spans 80 days.

	C 21	C 22	C 23	C 24	RMS
Difference in max* in 0°-45° (in counts [and in σs])	33 [1.14]	3 [0.11]	7 [0.41]	2 [0.14]	16.9 [0.61]
Distance between max in 0°-45° (in bins)	0	0	1	2	1.12
Difference in global max (in counts [and in σs])	33 [1.14]	27 [0.99]	7 [0.41]	9 [0.63]	22.1 [0.84]
Distance between start of cycle[†] (in bins)	3	3	7	3	4.4
Difference in total length of cycle (in days)	n/a	8	8	n/a	-

* “Max” refers to the maximum count. † See text for definition.

A.2 Timing

It will be tested whether a satisfactory agreement between the data and the overlapping of the two used Gaussians (Table 2) could arise randomly, or if it is indeed connected to the two planets' synodic period (Paragraph 2.1). For this, the periodic displacement between the two Gaussians is let to vary arbitrarily, and the agreement between the resulting predictions and the data is checked: To do so, while the actual average length between consecutive alignments is 3,634 days, its value is let to iterate between 2,000 and 5,000 days. For illustration, Fig.13 shows the expected distribution for a hypothetical length of 2,500. (Only the first 15,000 days are used in the tests.)

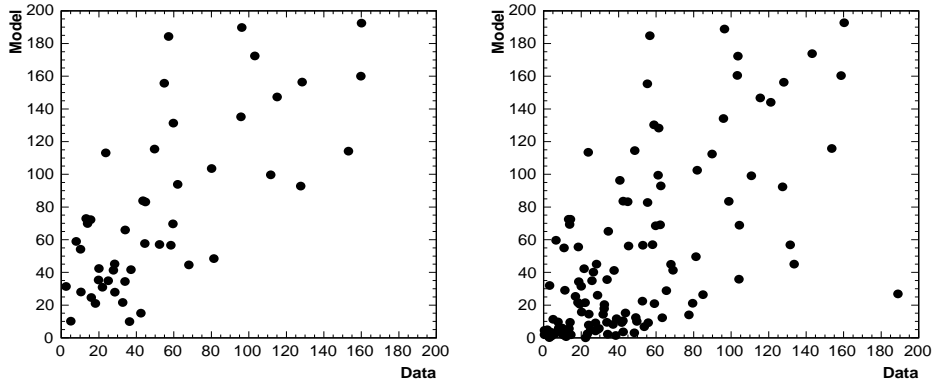


Figure 12: *Distribution of counts of flares in the prediction versus observations. Left: Within the range 0° - 45° of each cycle; 48 points. Right: For the whole time range; 121 points.*

We apply the Kolmogorov-Smirnov test using the ROOT[9] package, to check the compatibility of the data with the predicted distributions for each value of the time length.

Although including the dataset used for the derivation of the model should be avoided in the Kolmogorov-Smirnov test, it is assumed that in the present case the model was derived too indirectly from the distribution of cycle 21 (Paragraph 2.1), therefore it is appropriate to include all cycles in the test. Ideally, the test should be performed on unbinned data. For this, we perform the test both with the binning used in the rest of the analysis (80 days per bin) and with one bin per day. (In principle this introduces a source of uncertainty because of the need to change the constant of the Gaussians to match the new histogram's scale; however, the results from the two runs are almost identical, so this uncertainty was not incorporated in the calculations.)

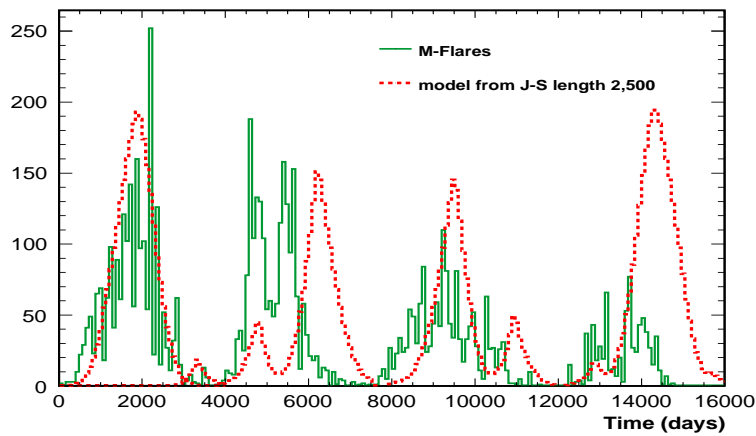


Figure 13: *An example prediction where the average length between the two planets' alignments would be 2,500 days.*

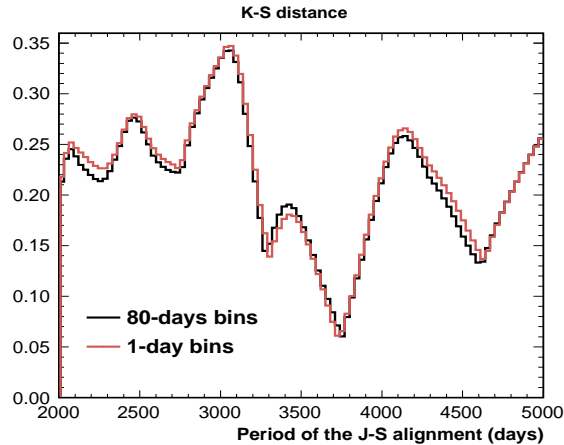


Figure 14: *Kolmogorov-Smirnov distances for varying numbers of the length between alignments, for data binned in 80 days (black) and with one bin per day (red).*

As seen in Fig.14, the tests with the two binnings show a well-defined global minimum at 3,710 and at 3,740 days respectively, close to the actual value for the average length between alignments (3,634), while at the same time no similarly strong minima occur for other lengths. In addition, Appendix B.3 calculates the uncertainty on the results due to dropping the adjustment term on the displacement during the iterations; the uncertainty is equal to 13.7%. This makes the results at the minimum and at the actual value lie less than 2.5 standard deviations away. Overall, the test supports the non-randomness of the proposed mechanism.

Finally, it can be noted that the chi-square test cannot be used here because of the many predicted empty bins and their importance. Still, ad hoc modifications on it for evading the empty bins result in similarly well-defined minima, in proximity to the actual value of the average length between alignments.

B Systematic uncertainties

B.1 Binning effects

Different choices of binning change the short-scale distribution of flares in each cycle, a fact which should be reflected in the model's degree of goodness. Re-deriving the two Gaussians for different binnings would add complication, since the fit used quasi-empirical constraints (Paragraph 2.1). Instead, we plot again the number of flares while varying the number of bins by ± 6 around the original number 50, in steps of 2; we calculate the chi-square over the number of degrees of freedom between the original prediction and each resulting data distribution; and we use the standard deviation from all seven results for the uncertainty value. In all cases we retained only the bins between $\pm 1,500$ days, for stability and to avoid empty bins. For illustration, the two extreme

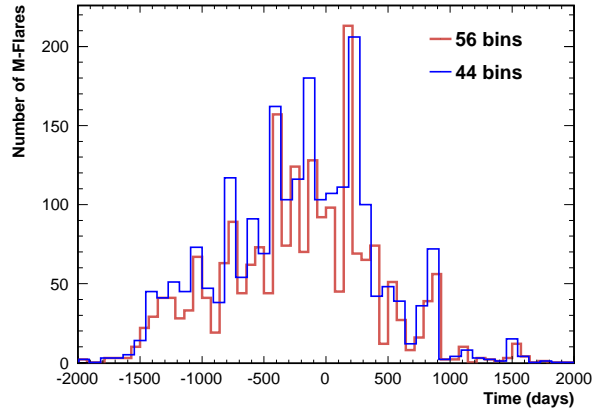


Figure 15: *Distribution of flares in cycle 21 for the two extreme tested numbers of bins.*

binning are plotted in Fig.15.

The resulting uncertainty is 13.5% on the original χ^2/ndof . This value is applicable to each bin of the model in all cycles.

B.2 Fluctuations of the established length

In Paragraph 2.2 a hypothesis was made about calculating the middle of a cycle, based on the average lengths of the two contributing effects (Eq.1):

$$[\text{displacement}] = D + (\langle 11y \rangle - \langle L_{JS} \rangle) + \frac{L_{JS} - \langle L_{JS} \rangle}{2}$$

The records of the average “11 year” period show a deviation of 10%, while the average duration between two alignments has a natural fluctuation of 2%. However, the dates of the alignments are known exactly, while also the deviation from their average value is taken into account in the formula (in the last term). Therefore, the only uncertainty entering this calculation comes from the “11 year” average. Its uncertainty of 10% is propagated to the value of the average difference of the two effects.

As described in Paragraph 2.1, the model is constructed by selecting the lower value among the two Gaussians in each bin. Therefore the uncertainty is found by centering the established Gaussian on its two extreme positions for each cycle (i.e. the position calculated from Eq.1 ± 39 days) and taking the difference from the nominal value of the model in each bin. The resulting uncertainties are shown in Fig.16. They are applicable to each bin of the model whenever Eq.1 is used, except on cycle 21.

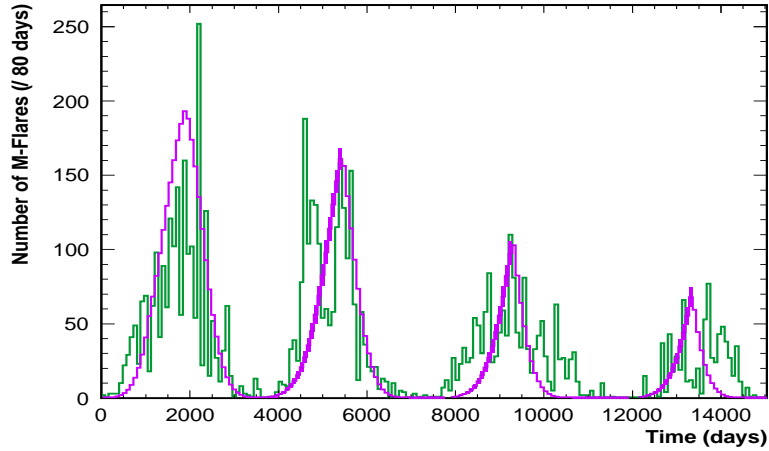


Figure 16: All flare observations for the last four cycles (green), overlaid with the prediction distribution (violet). The systematic uncertainty due to fluctuations of the established length is shown as violet shade. (This source of uncertainty does not apply to cycle 21.)

B.3 Synodic period without adjustment

In Appendix A.2 statistical tests are performed by letting the displacement between the two Gaussians vary arbitrarily. In that case the increase in the displacement is constant, while in the actual model the increase is adjusted in each cycle according to the time between the planets' alignments (Paragraph 2.2, Eq.1). Therefore, dropping the adjustment term introduces a source of systematic error in the distributions entering the statistical tests.

In order to quantify this uncertainty, we use the value of the Kolmogorov-Smirnov distance for the comparison of the model to the observations, with and without the adjustment term in Eq.1. The resulting change is 13.7%, and is used as systematic uncertainty on the results of Appendix A.2.